Chapter 3

Supercontinuum generation by fission of higher-order solitons in photonic crystal fibers

Photonic crystal fibers (PCF) are currently a topic of high interest because of their unusual optical properties and their potential for important applications. The refractive index difference between the core and the holey cladding provides a very strong specifically controlled waveguide contribution to dispersion. Therefore the PCFs possess peculiar optical properties such as infinitely-single-mode guiding [2, 6, 78] or shift of zero-dispersion wavelength [6, 7, 8]. As a result new features in nonlinear optical effects arise that can not be observed in standard optical fibers. One such phenomenon is the generation of an extremely broadband supercontinuum (SC) covering more than two octaves strarting from low-energy ($\sim$1 nJ) pulses with an initial duration τ_0=100 fs [8]. The analogous effect has also been observed in tapered fibers [10]. In comparison, SC generation in standard fibers

requires more than two orders of magnitude higher initial peak intensities I_0 [12, 79, 14]. The dramatic spectral broadening of relatively low-intensity pulses in PCF's is an interesting phenomenon and has already been used in several fascinating applications, for example in frequency metrology as described in the introduction. SC generated in a PCF is also an excellent source for optical coherence tomography with ultrahigh resolution in biological tissues [80]. Furthermore, there is a large potential for numerous applications such as pulse compression, laser spectroscopy, all-optical telecommunication, dispersion measurements, sensor technique and others. Doped fibers can be applied as element of laser systems [81], with large mode area being especially useful for the generation of intense pulses [82].

3.1 Solitons and broadening in different dispersion regimes

The formation of a broad spectrum by the interaction of intense pulses with matter has been discovered already in the seventies, first in condensed matter [57], and later also in single-mode fibers (for an overview see [13]). The physical origin of this effect is a refractive index change by the electric field $\Delta n = n_2 I(t)$, where $I(t)$ is the intensity and n_2 the nonlinear refractive index. As a result a time-dependent phase is induced which implies the generation of new spectral components around the input frequency ω_0 with maximum spectral width $\Delta\omega_{SPM}/\omega_0 = 1.39 n_2 I_0 L/\tau_0 c$ [50], where L is the propagation length. Normal group-velocity dispersion limits this width while in the anomalous dispersion region the balance of GVD and SPM leads to

the formation of solitons. At higher amplitudes a higher-order soliton with soliton number N is formed. Such a bounded N-soliton undergoes periodic narrowing and broadening during propagation. Higher-order nonlinear and dispersive effects lead to a break-up of N-solitons into their constituent 1-solitons [84] and the emission of blue-shifted <u>non-solitonic radiation</u> (NSR) [63, 65, 64, 87] (for an overview see [50]).

As will be shown the low-intensity spectral broadening observed in PCF's is caused by a different mechanism and can not be explained by the effect of SPM for pulses in the range of 1 nJ and 100 fs duration. To study the basic mechanism of SC in PCF's we solved the nonlinear evolution equation (2.66) with the method for the determination of the eigenvalue $\beta(\omega)$ in a PCF as described in Section 2.2 for different input and PCF parameters. First we solve the pulse propagation equation for a PCF with $\Lambda = 1.5$ μm, $d = 1.3$ μm and the zero dispersion frequency $\omega_{ZD} = 2.66$ fs^{-1} (λ_{ZD}=710 nm) for pulses with large duration (FWHM) $\tau_0 = 100$ fs and a relatively low intensity $I_0 = \epsilon_0 n(\omega) c E^2 / 2 = P_0 / S_1 = 0.6$ TW/cm^2. In order to study the crucial role of the specific PCF dispersion, we consider the propagation of pulses with different initial frequencies presented in Fig. 3.1. For the parameters in Fig. 3.1 the initial frequency $\omega_0 = 0.6\omega_{ZD}$ is deep in the anomalous region, the magnitude of the negative GVD parameter D is relatively large and the TOD parameter is very small. The soliton number for these parameters is N=4.3. The solution presented in Fig. 3.1 for $\omega = 0.6\omega_{ZD}$ can be identified as a bounded fourth-order soliton which is also well described by the analytical solution of the NSE with typical periodic evolution with the propagation length and splitting into three distinct peaks which merge again later [50]. At the initial frequency $\omega_0 = 1.07\omega_{ZD}$ and $\omega_0 = 1.37\omega_{ZD}$ in the normal
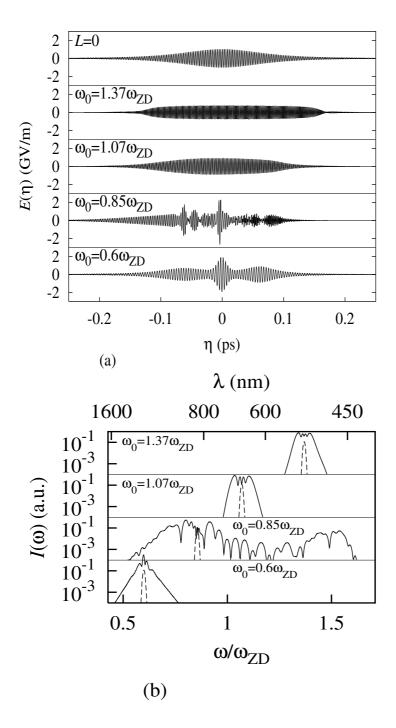
Figure 3.1: Output pulse shapes (a) and spectra (b) for L=15 mm, I_0=0.6 TW/cm^2, τ_0=100 fs and different input frequencies as indicated. Initial spectra (dashed, scaled for clarity here and hereafter) and pulse shape [$L = 0$ for $\omega_0 = 0.85\omega_{ZD}$ in (a)] are also presented.

dispersion range, spectral broadening typical for SPM can be found, with a spectral width $\Delta\omega/\omega = 0.06$ which agrees approximately with the above given maximum width 0.07. However as can be seen for $\omega_0 = 0.85\omega_{ZD}$ for the same input intensity and pulse duration a qualitatively different behavior arises: the spectrum shows more than one order of magnitude larger FWHM width (Fig. 3.1).

3.2   Comparison of spectral broadening for different input pulse durations

To study the physical reason for such surprising behavior illustrated in Fig. 3.2(b), the evolution of the spectra (solid curves) and the spectral phases (dotted curves) is plotted while in Fig. 3.2(a) the evolution of temporal shapes is shown for the same parameters as in Fig. 3.1 with initial central frequency $\omega_0 = 0.85\omega_{ZD}$ (initial wavelength $\lambda_0 = 830$ nm). After about 10 mm the spectrum is still relatively narrow , but with further evolution it broadens significantly with large extension from IR to the violet and a width of more than 500 nm. The theoretical prediction presented in Fig. 3.2(b) is in good agreement with experimental measurements for the same input pulse parameters reported in Ref. [8]. Comparison with the result of a recent study [83] also shows good qualitative agreement in the final spectra, albeit for different fiber geometry. The evolution of the temporal shape presented in Fig. 3.2(a) shows that the pulse successively splits into finally seven ultra-short peaks moving with different velocities and shapes which do not change their form over a long distance. It is impossible to explain the extremely
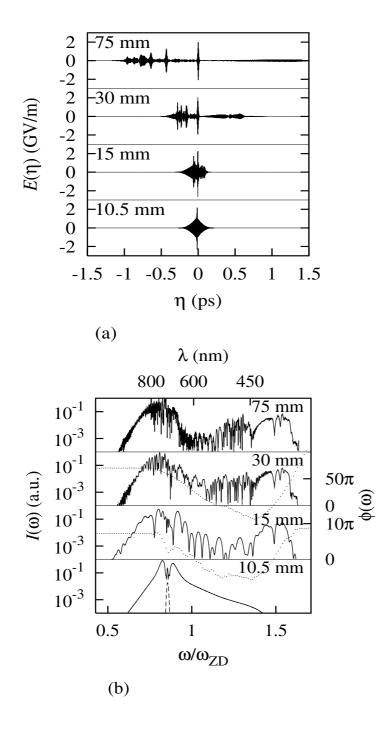
(a)

(b)

Figure 3.2: Output pulse shape (a) and spectrum (b) for $\omega_0 = 0.85\omega_{ZD}$, I_0=0.6 TW/cm^2, τ_0=100 fs for different propagation lengths as indicated. Spectral phases are shown by dotted curves for z=15 mm and 30 mm.
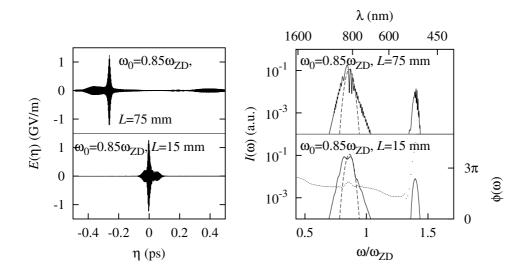
Figure 3.3: Evolution of output pulse shape (a) and spectrum (b) for $\omega = 0.85\omega_{ZD}$, I_0=0.6 TW/cm^2, τ_0=17.5 fs. Dotted curve shows spectral phase for z=15 mm.

broad spectrum for the rather long pulses with a relatively small intensity by the effect of SPM. As discussed above, the largest spectral broadening by SPM is given by [50] $\Delta\omega_{SPM}/\omega_0 = 1.39 n_2 I_0 L/(\tau_0 c) = 0.07$ for the input pulse parameters given in the caption of Fig. 3.2, while we obtained more than one order of magnitude broader spectrum. Additionally, we find a surprising result if we consider the spectral broadening of a shorter pulse with the same intensity, as shown in Fig. 3.3. As can be seen in Fig. 3.3(b), for $\omega_0 = 0.85\omega_{ZD}$ the spectral width of about 50 nm generated by a 17.5 fs pulse is ten times smaller compared with the 100-fs-pulse case in Fig. 3.2. This much narrower spectrum is in direct contrast to the behavior of SPM-induced broadening. In the SPM, corresponding the expression (2.42) for $\Delta\omega_{SPM}/\omega_0$, an about 6 times shorter pulse should yield a correspondingly larger width. The temporal shape presented in Fig. 3.3(a), upper section shows the forma-

tion of a single short spike together with background radiation. While the spike does not change its form during propagation from 15 mm to 75 mm, the background radiation becomes temporally broadened.

3.3 Interpretation of the results

The behavior of SC generation in PCF's described above is qualitatively different from SPM-induced broadening and requires a careful study of its physical origin. Note that the considered input frequency $0.85\omega_{ZD}$ in Fig. 3.2 and Fig. 3.3 is in the anomalous region and, therefore, soliton dynamics plays a crucial role in the propagation. The input parameters in Fig. 3.2 imply the formation of a higher-order soliton [50] with a soliton number $N = \sqrt{n_2 I_0 \omega_0 \tau_0^2 L/|D|c} = 7.8$. Higher-order solitons of the NSE show periodic changes with propagation and can not explain the effects described above. But in a PCF higher-order dispersion effects are stronger than in standard fibers and play a much more significant role in pulse propagation. Previous studies [84, 63, 64, 65] of the perturbed NSE, taking into account positive TOD, predict the following behavior: A higher-order soliton with number N splits into N pulses with different red-shifted central frequencies and different group velocities [84]. After the fission every pulse emits nonsolitonic radiation phase-matched to the corresponding pulse [64, 65] while simultaneously moving to IR until the stability is reached [65]. The shift of the soliton frequency due to Raman effect plays a minor role, because it requires significantly longer propagation [85, 86]. Although the perturbed NSE is not valid for the propagation phenomena illustrated in Fig. 3.2 and the spectral broadening and shifts in standard fibers are two orders of mag-

nitude smaller, the analogous effects in PCF's can be readily identified as the physical origin of the SC generation. The amplitudes and durations of the separated spikes in Fig. 3.2(a) satisfy the relation for a fundamental soliton [50]. To corroborate the soliton nature of these spikes, we simulated the propagation of every separated pulse over a distance of 75 mm and did not found any change in shape and spectrum during propagation. For the same conditions a low-intense pulse would spread by a factor of 200. The higher-order soliton splits into fundamental red-shifted 1-solitons and loses energy by emitting blue-shifted NSR. This process is illustrated by the scheme in Fig. 3.4. The pulse durations of the 1-solitons are determined approximately by $\tau_n = \tau_0/\zeta_n$ [84] and their frequency-shift by $\Delta\omega_s \approx 7/\tau_n$ [63] where $\zeta_n = 2A_0 - n, \quad n = 1, 2 \ldots N$ are determined by the eigenvalues of the NSE. This scenario explains the numerically calculated features in Fig. 3.2 and the given rough analytical estimates for τ_n and $\Delta\omega_s$ are supported by our numerical computations, with acceptable deviations. All spectral components of each soliton are phase-locked and the solitons preserve their shape and spectrum in collisions. The calculated spectrum of the three isolated strongest solitons show a red-shift with central frequencies at $0.87\omega_0$, $0.93\omega_0$ and $0.97\omega_0$, and its velocities are close to the corresponding group velocities. The phases of a soliton at frequency ω_s in its moving frame, and that of the non-solitonic radiation at ω in the same frame ,are given by, respectively,

$$\phi_s(\omega_s) = \beta(\omega_s)L + n_2 I \omega_s L/(2c) - \omega_s L/v_s \qquad (3.1)$$

and

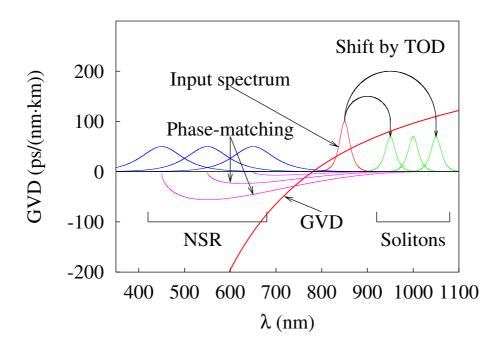$$\phi_r(\omega) = \beta(\omega) - \omega L/v_s \qquad (3.2)$$

Figure 3.4: Scheme of a SC generation by fission of higher-order solitons. Thick red line is GVD for a PCF with core radius 2.5 μm. Spectra of NSR, solitons, and input pulse are presented by blue, green, and thin red lines, respectively. The phase mismatch between solitons and NSR is presented by violet lines.

where $v_s = [\partial\beta/\partial\omega(\omega_s)]^{-1}$ is the group velocity of the soliton. In Fig. 3.5 in the curves 3 and 4 the phase difference $\Delta\phi = \phi_s - \phi_r$ for the strongest and weakest soliton with respect to its corresponding non-solitonic radiation is presented together with the dispersion lines for fused silica and the PCF under consideration.

The strongest soliton is phase-matched with non-solitonic radiation at 400 nm and the weakest at 550 nm. Due to the presence of several solitons with different frequencies, distinct spectral fractions arise and therefore a broad spectrum is generated in the intermediate range between 430 nm to 550 nm. The spectrum in the range between 550 nm and 700 nm arises as a result of nonlinear interactions between the solitons and the blue-shifted continuum. The phase relations discussed above are supported by the numerically calculated spectral phases of the pulses $\tilde{\phi}$. In the dotted lines in Fig. 3.2 the modified phase $\tilde{\phi}(\omega) = \phi(\omega) - \omega L(1/v_s - 1/c)$ is plotted. As can be seen, the blue-shifted part of the radiation with highest frequencies is indeed phase-matched with the most intense fundamental soliton, and analogous phase relations can be found for the other solitons. Now the result in Fig. 3.3 for a shorter input pulse but a narrower output spectrum can be explained. Since for the smaller pulse duration the soliton number with $N = 1.5$ corresponds to one fundamental soliton, no soliton fission can occur and only an isolated blue-shifted side peak is generated.

SC's by fission of higher-order solitons can also be generated by shorter pulses, but the necessary intensity for a short pulse is higher. Thus Fig. 3.6 demonstrates that a 10-fs pulse, but with 5.5 times higher input intensity generates a SC in a photonic fiber with $\Lambda = 1.65$ μm and $d = 1.3$ μm (corresponding $\lambda_{ZD} = 767$ nm and $N = 2.87$) through soliton fission. The temporal
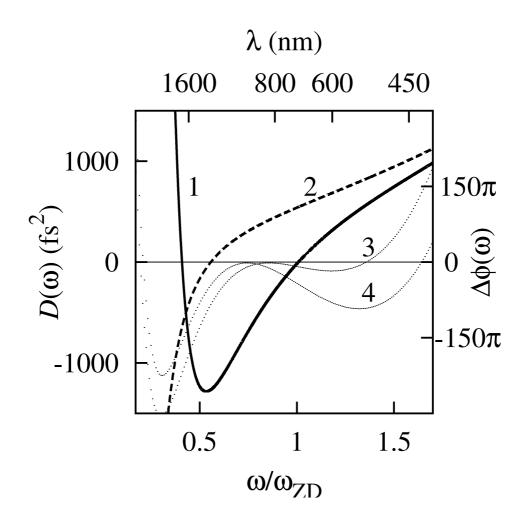
Figure 3.5: The GVD coefficient $L\partial^2\beta/\partial\omega^2$ in PCF with Λ=1.5 μm, d=1.3 μm (curve 1) in comparison with the GVD coefficient for bulk silica (curve 2) and phase mismatch for the strongest (curve 3) and the weakest (curve 4) solitons to their corresponding radiation for the conditions of Fig. 3.2. Fiber length L is 15 mm.
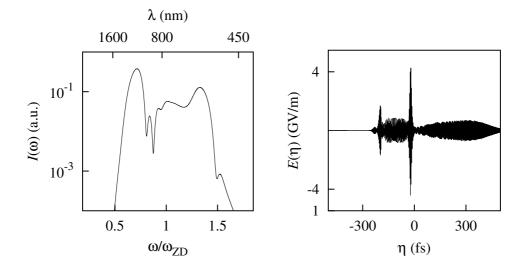
Figure 3.6: Output pulse shape (right) and spectrum (left) for L=15 mm, I_0=3.3 TW/cm^2, τ_0=10 fs, $\omega_0 = 0.92\omega_{ZD}$.

shape (right) shows the fission into two solitons with their blueshifted emission as the reason for SC generation in Fig. 3.6 (left). The spectrum covers the range 500–1300 nm and agrees with experimental observations [18] for the same parameters.

3.4 Experimental evidence for supercontinuum generation by fission of higher-order solitons

The experimental results shown here are a result of the collaboration with the experimental group in the MBI of Dr. U. Griebner, Dr. N. Zhavoronkov, Dr. D. Nickel and Dr. G. Korn. The spectra shown by black lines in Fig. 3.7(a),(b) where measured by that group. The fibers were produced by

experimentalists from the University of Bath, group of Prof. P. St. J. Russel, Dr. J. C. Knight, and Dr. W. J. W. Wadsworth. In the experiments, a cavity dumped beam from a Ti:sapphire oscillator with a pair of prisms incorporated for GVD control was used. To adjust the wavelength of radiation as well as its bandwidth a variable slit was introduced into the dispersive arm of the cavity. Almost transform-limited pulses centered at 850 or 807 nm with pulse durations of 29 and 100 fs for both wavelengths were generated. For these wavelengths the GVD is anomalous in our PCF. One can continuously change the repetition rate keeping the pulse energy constant but decreasing the average power to prevent overheating of the fiber. The pulse energy could be changed quite easily by altering the RF power delivered to the dumper. Furthermore, the laser is not sensitive to feedback from the fiber tip which could interrupt the mode-locking in the case of an ordinary fs-oscillator. To keep the pulses spectrally limited after passing through the focusing microscope objective a combination of a fused-silica pair of prism and negative-GVD ($\sim$40 fs^2 per bounce) mirrors were used. The PCF's are air-silica 40-cm-long microstructured fibers with core diameters of $d =$1.6 and 2.5 μm and zero-dispersion wavelengths of 670 and 790 nm, respectively. The spectra generated in the fibers covered the range up to 350 nm – 1600 nm, and were measured with an optical spectrum analyzer (ANDO AQ-6315A). The peak intensity in the fundamental mode inside the fiber was estimated from the measured power behind the fiber. Part of the launched power was guided in cladding or higher-order modes and formed the undepleted fundamental peak. This fraction was determined from the experimental spectra [Fig. 3.7(a),(b)], and the intensities were correspondingly corrected. Comparison of theoretical and experimental spectra reveals good agreement in width and

characteristic features and allows to identify the physical mechanism for SC in PCF's.

Now we want to study how the evolution of spectra depends on the input intensity. In Fig. 3.7(a) the calculated output spectra for a PCF with core-diameter of 2.5 μm is presented for a 29 fs input pulse with three different peak intensities 27 GW/cm^2, 0.24 TW/cm^2 and 0.7 TW/cm^2, centered at 850 nm, and in Fig. 3.7(b) the same is shown for a 100 fs pulse. Apparently, for an intensity of 0.24 TW/cm^2 [middle section of Fig. 3.7(a)] the spectrum of the 29 fs pulse is slightly broadened with an additional blue-shifted side-peak, while the 100 fs pulse generates a SC extending from 500 nm to 1300 nm. For a three times higher intensity the spectral width of both pulses increases, but the spectrum of the longer pulse is flatter. As becomes evident particularly by comparison of the middle section of Fig. 3.7(a) and (b), the results are again in direct contrast with the behavior of spectral broadening by SPM: a larger bandwidth is generated for a longer pulse with the same input intensity.

The temporal shapes after propagation through the fiber are presented in Fig. 3.8(a) and (b). The input parameters in the middle section of Fig. 3.8(b),(d) and Fig. 3.7(b) imply the formation of a N=6 soliton (A_0=5.69); the fission of this pulse into 6 short fundamental solitons can be seen in Fig. 3.8(b) together with a longer pulse which is the blue-shifted NSR. The two shortest and most intense solitons have durations of 12 and 15 fs and red-shifts of $-0.17\omega_0$ and $-0.09\omega_0$. The blue-shifted part of the continuum in Fig. 3.7(b) is phase-matched to the corresponding solitons. In Fig. 3.8(d) the phase difference $\Delta\phi$ as given in (3.1) and (3.2) for the most intense soliton (solid), the third strongest soliton(long-dashed) and the weakest soliton
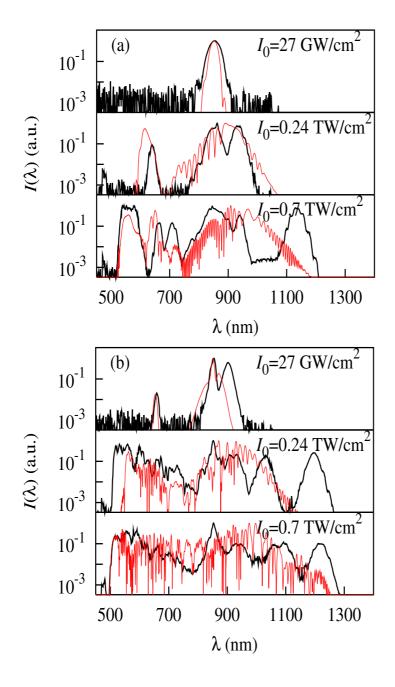
Figure 3.7: Experimental (black) and theoretical (red) spectra for input pulse durations of 29 fs (a) and 100 fs (b). The core diameter of the PCF is 2.5 μm and the input wavelength is 850 nm.
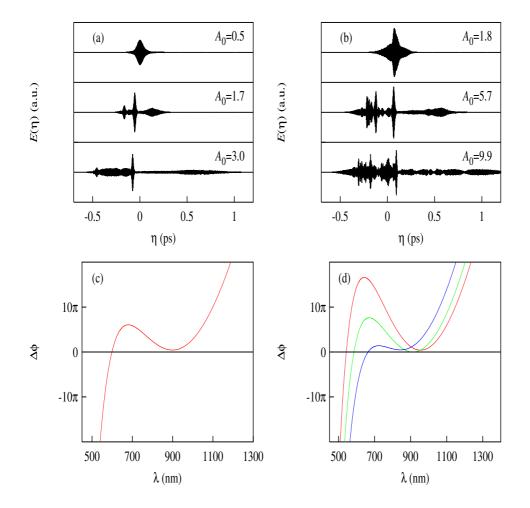
Figure 3.8: Pulse shapes (a),(b) and phase difference (c),(d) for $\tau_0 = 29$ fs (a),(c) and $\tau_0 = 100$ fs (b),(d) in PCF with 2.5-μm core diameter. Input wavelength is 850 nm. In (a) and (b), theoretical pulse shapes are presented together with the corresponding soliton parameter A_0. In (c) and (d), phase mismatch is shown for the strongest (red curves), second strongest (green curve) and weakest (blue curve) soliton.

(short-dashed) with respect to their NSR are presented. Phase-matching $\Delta\phi = 0$ is realized for these solitons at 542, 586, and 664 nm, respectively. Thus every soliton emits radiation only at a certain frequency interval and distinct spectral fractions of NSR arise covering the range from 500 to 850 nm. In contrast, the soliton number for the 29 fs pulse [illustrated in the middle section of Fig. 3.8(a),(c) and Fig. 3.7(a)] is $N=2$ ($A_0=1.7$). Therefore, two solitons are formed [Fig. 3.8(a) middle]. One of them is weak, long and its frequency shift is small. The stronger soliton with central wavelength 898 nm produces NSR only in a small isolated interval around 600 nm, as predicted by the phasematching $\Delta\phi = 0$ in Fig. 3.8(c). This explains why the shorter 29 fs pulse with the same peak intensity yields a narrower spectrum, depicted in Fig. 3.7(a), than the longer 100 fs pulse. For the lower intensity, no solitons emerge ($A_0 = 0.5$) for the 29-fs input pulse, as can be seen in the top sections of Fig. 3.7(a) and Fig. 3.8(a), while for the 100-fs input pulse one red-shifted soliton is formed [top section of Fig. 3.7(b) and Fig. 3.8(b)] together with blue-shifted radiation. This radiation is seen as a small peak at $\sim$650 nm in the top section of Fig. 3.7(b). With increasing intensity in the bottom sections in Fig. 3.7 the short 29 fs pulse forms $N=3$ solitons and can also generate a broad spectrum, but the spectrum of the 100 fs pulse with the same intensity is much smoother due to the fission into $\sim$10 fundamental solitons. The fast oscillations in the numerically calculated spectrum arise due to the interference of the different solitons.